COMMUNICATION

Organic Nanohybrids for Fast and Sustainable Energy Storage

Minah Lee, Jihyun Hong, Haegyeom Kim, Hee-Dae Lim, Sung Baek Cho, Kisuk Kang, and Chan Beum Park**

With the emerging demand for large-scale energy-storing batteries concerns have been raised regarding the consumption of a large volume of material resources in the fabrication of batteries mostly based on transition metals. As such, requests for greener and naturally abundant materials in energy storage have been escalating recently in society.[1,2] In this respect, organic chemicals available in natural resources are promising alternatives.[3] The minimal environmental footprint as well as distinctive material properties such as light weight, flexibility, and chemical tunability makes them beneficial as an electrode material in large-scale batteries. In particular, the use of bio-inspired organic electrodes that imitate energy metabolisms,[4] such as respiration and photosynthesis, will enable a design of more sustainable batteries. For example, the electro-active carbonyl compounds mimicking biological quinone cofactors that can be obtained from biomass through eco-friendly processes are intriguing candidates for such electrode materials.[5–7] Also, flavin-based electrodes that function through the imitation of the cellular energy transduction mechanism are promising candidates we recently introduced.[8]

Despite the recent advances in organic-based electrode materials,[9] critical obstacles still exist for their practical use in energy storage. Most organic-based electrodes suffer from rapid capacity fading upon cycling due to the dissolution of active organic chemicals into organic electrolytes and show poor power capability because of the low electronic conductivity.[5,10,11] Several strategies have been suggested to resolve the dissolution issue, such as covalent attachment of redox molecules to substrates,[12] polymerization of active compound,[13–15] optimization of molecular structure,[16] and the use of solid electrolytes.[17] Some recent works used organic composites as high power electrodes, but active material loaded in the electrode was quite low (less than 10%).[18,19] While these recent achievements bring the use of naturally benign organic materials a step closer to the practical battery systems, a strategy to enhance cyclic stability and power capability simultaneously in a simple way that can be generally applied to organic-based electrode materials is still lacking.

Here, we present a novel and general approach for the development of organic electrodes in which active organic materials with aromatic redox centers are immobilized to conductive scaffolds through non-covalent bonding yielding a self-standing and flexible nanohybrid organic electrode. The nanohybrid organic electrodes exhibited surprisingly high capacity retention of nearly no capacity reduction after 100 cycles with unprecedentedly high power capability. As a model redox-active chemical, flavin molecules were employed (Figure S1, Supporting Information, **Scheme 1**). The aromatic structure of flavin molecules allows them to strongly anchor to the hydrophobic surfaces of conductive single-walled carbon nanotubes (SWNTs) scaffolds via π–π interactions without disruption of their redox-active properties. Regarding a gravimetric energy density, lumiflavine (LF) that has minimal molecular structure among various flavin molecules was selected as the active material. We expected that the LF-immobilized SWNTs (LF-SWNT) nanohybrid would mitigate the common problems of conventional organic electrode based on the following hypotheses (Scheme 1):

i. Tethering the electro-active molecules on the surface of SWNTs through molecular rearrangement of LF from crystalline bulk particles into a nano-layer will allow a molecular level contact between the active materials and the conductive scaffold. This will enhance both conductivity and lithium-ion accessibility of the electrode.
ii. Non-covalent immobilization of the redox molecules via π–π interactions on the SWNTs scaffold will suppress the dissolution of the active chemicals into liquid electrolyte.
iii. In the LF-SWNT nanohybrid electrode, the self-standing SWNT network will function as binder and current collector. Consequently, the nanohybrid electrode will not lose the practical energy density arising from the additional weight of binder, conductive agents, and the current collector.

LF-SWNT nanohybrids can be obtained by simply mixing SWNTs and LF in a solvent of intermediate polarity, accompanied with continuous homogenization of the solution. Briefly, SWNTs and LF powder were added into acetone and the mixed solution was homogenized for 15 min, followed by sonication for 8 hours at room temperature. Subsequent vacuum filtration of the solution formed a thin film that is removable from

M. Lee,[+] Prof. C. B. Park
Department of Materials Science and Engineering
Korea Advanced Institute of Science and Technology
Daejeon 305–701, Republic of Korea
E-mail: parkcb@kaist.ac.kr
J. Hong,[+] H. Kim, H.-D. Lim, Prof. K. Kang
Center for Nanoparticle Research
Institute for Basic Science (IBS)
Department of Materials Science and Engineering
Research Institute of Advanced Materials (RIAM),
Seoul National University
Seoul 151–742, Republic of Korea
E-mail: matlgen1@snu.ac.kr
Dr. S. B. Cho
Agency for Defense Development
Daejeon 305–152, Republic of Korea
[+]These authors contributed equally to this work

DOI: 10.1002/adma.201305005

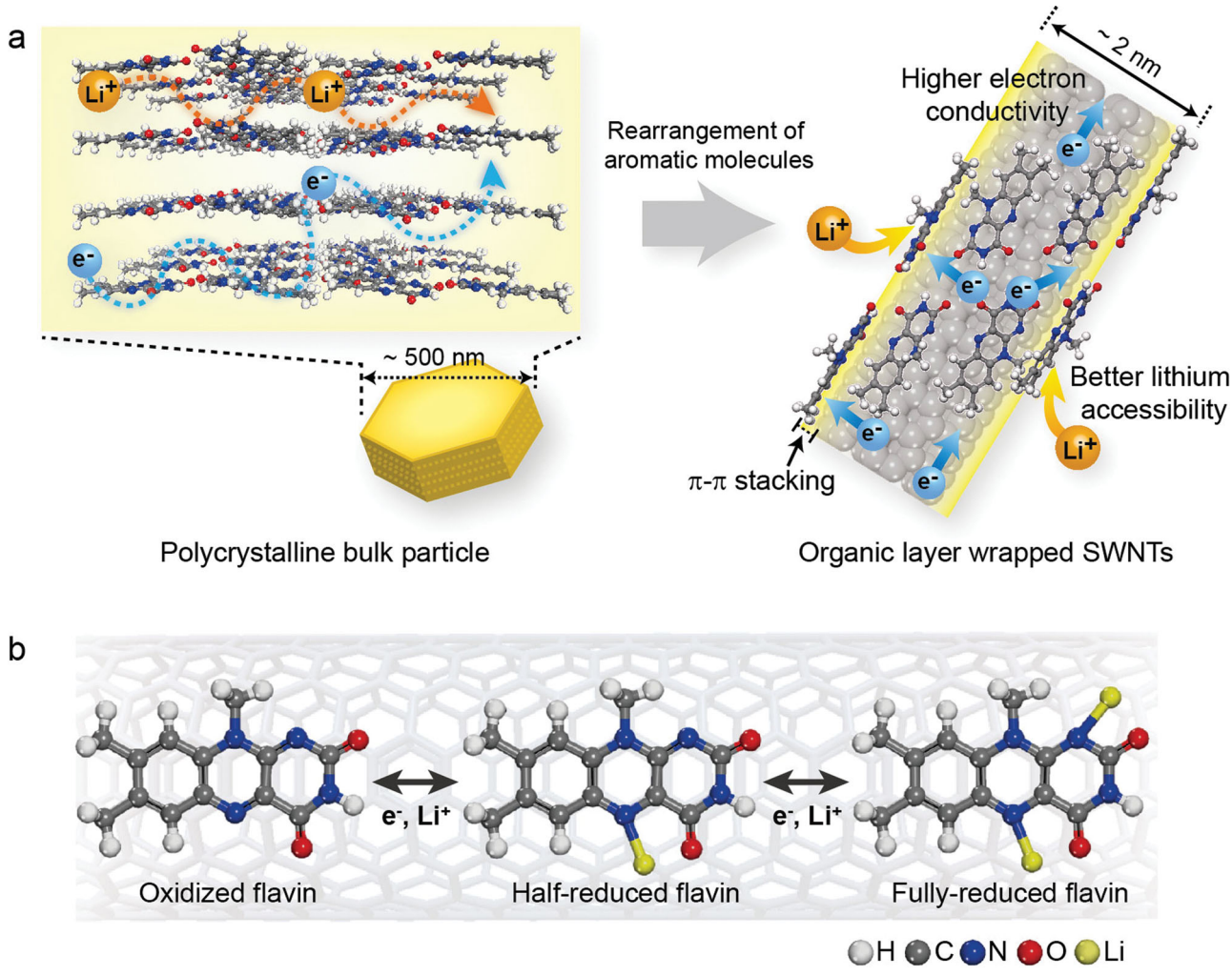

Scheme 1. a. Nanohybridization strategy of aromatic redox molecules with SWNTs for high performance lithium rechargeable batteries. The organic nanolayer on SWNTs formed via disassembly of crystalline structure of LF upon the immobilization with SWNTs can have higher electron conductivity and better lithium accessibility than the polycrystalline bulk particle. b. The energy storage mechanism of flavin in lithium rechargeable batteries via two lithium-ion coupled two electron transfer reaction.

the membrane, resulting in a flexible, free-standing LF-SWNT paper with a thickness of approximately 15 μm (**Figure 1**a,b). As the LF-SWNT papers are mechanically robust and electrically conductive, they can be directly used as electrodes without any binder or additives during electrochemical cell preparation.

We investigated the morphologies of LF-SWNT nanohybrids using electron microscopes. The TEM image of LF-SWNT in Figure 1d reveals the presence of amorphous layers on the sidewalls of SWNTs, which were not present on the pristine SWNTs (Figure 1c). Previously, Ju et al. and Tummala et al. reported that flavin derivatives having an isoalloxazine ring system can densely wrap around SWNTs in a helical pattern through concentric π–π interactions.[20–22] According to our SEM images, LF-SWNT was composed of a highly intertwined network of nanofibers (Figure 1f), while the pristine LF existed in the form of microparticles (Figure 1e). This indicates the disappearance of long-range crystalline ordering of LF molecules and their reorganization on SWNTs through hybridization. We further confirmed the disassembly of pristine LF crystal after the immobilization by comparing the electron diffraction patterns of LF, LF-SWNT, and SWNTs, respectively (Figure 1g–i).

The hybridization of LF and SWNTs was further examined using multiple spectroscopic analyses. The comparison of XPS survey spectra for SWNTs, LF, and LF-SWNT nanohybrids revealed that N1s peak around 400 eV, which originated from LF, is clearly present in LF-SWNT, while it is not detected in pristine SWNTs (**Figure 2**a). The existence of LF in the nanohybrids is also confirmed by the appearance of new peaks in the FTIR spectroscopic spectrum at 1548, 1583, 1662, and 1709 cm^{-1} (Figure 2b). The new peaks are attributed to C=N and C=O bonds in the adsorbed LF.[23] Note that there were negligible spectral changes of LF after their hybridization with SWNTs, which suggests that such non-covalent functionalization can preserve the chemical structure of the redox-active diazabutadiene motif (N_5-C_{4a}-C_{10a}-N_1) in LF. We observed π–π interactions between aromatic LF molecules and the sidewalls of SWNTs using Raman spectroscopy. The G-band of SWNTs

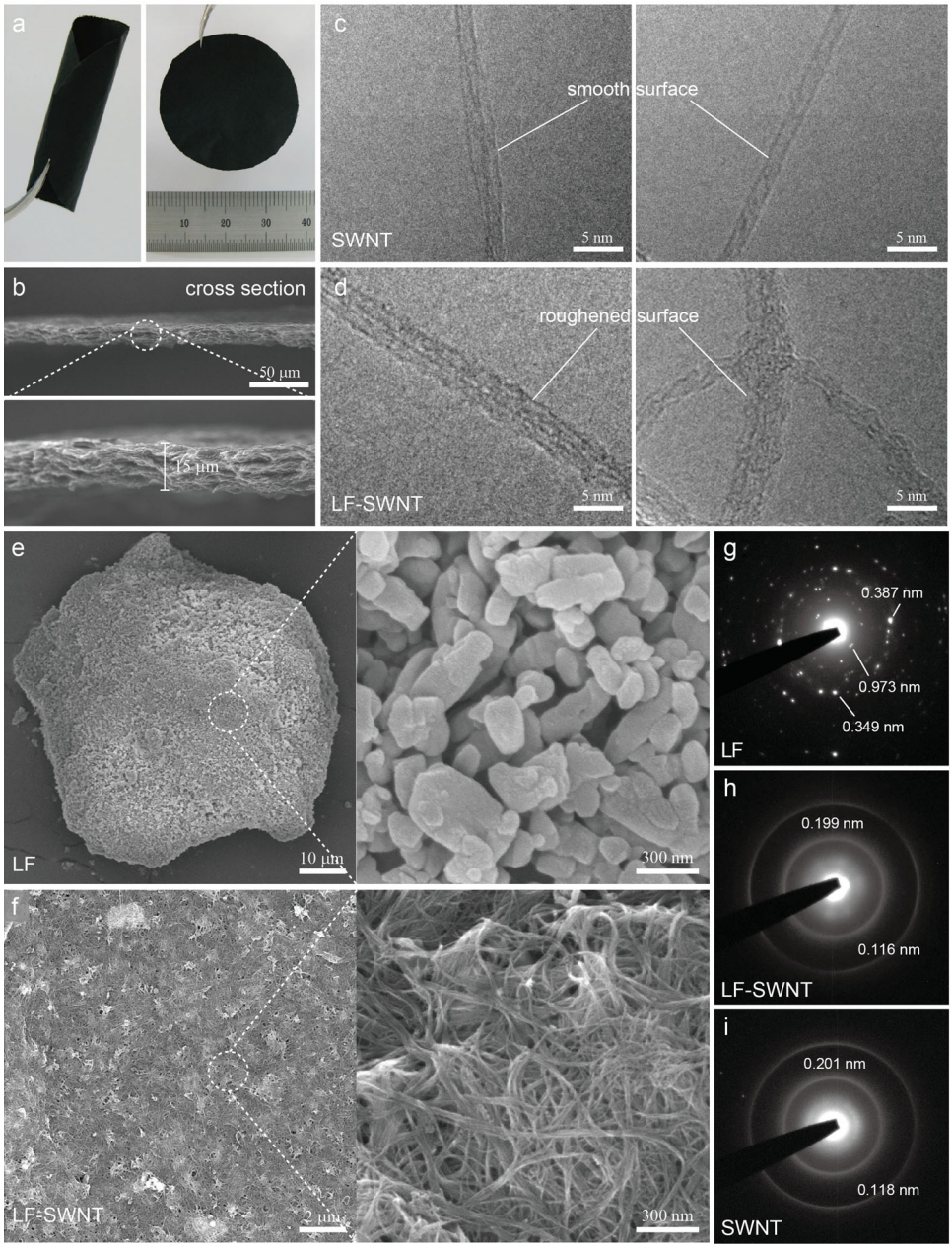

Figure 1. a. Photograph of flexible free-standing LF-SWNT electrodes. b. Cross-sectional SEM images of LF-SWNT c,d. TEM images of SWNTs and LF-SWNT. e,f. SEM images of LF-SWNT and LF. g,h,i. Electron diffraction patterns of SWNTs, LF-SWNT, and LF. The disappearance of the diffraction patterns in LF-SWNT indicates the disassembly of the crystalline structure of LF upon the immobilization.

after the hybridization was up-shifted by 4 cm^{-1} compared to that of pristine SWNTs (Figure 2c). Also, the Raman RBM band in the LF-adsorbed SWNTs showed higher frequency shifts in comparison with pristine SWNTs (Figure 2c, inset). The up-shifts of the Raman spectrum for SWNTs stem from the changes in the number of π-electrons of SWNTs,[24,25] which strongly indicates π–π interactions between SWNTs and aromatic molecules. Our thermogravimetric analysis (TGA) revealed that the nanohybrids have reasonable thermal stability at around 300 °C (Figure S2). Based on the weight loss in the range from 300 to 400 °C for LF-SWNT (~33%) and LF (~81%), we estimated the content of LF between 40–50% in the hybrid composite. According to the elemental analysis of LF-SWNT nanohybrids (N: 9.96 wt%), the amount of LF in the nanohybrid was approximately 45 wt% (Table S1).

We evaluated electrochemical performance of LF-SWNT nanohybrids as a cathode material in a lithium cell (**Figure 3**, a–e). Figure 3a and 3b present the characteristic electrochemical profiles of LF and LF-SWNT, respectively. Note that the capacity from SWNTs was negligible considering the high discharge

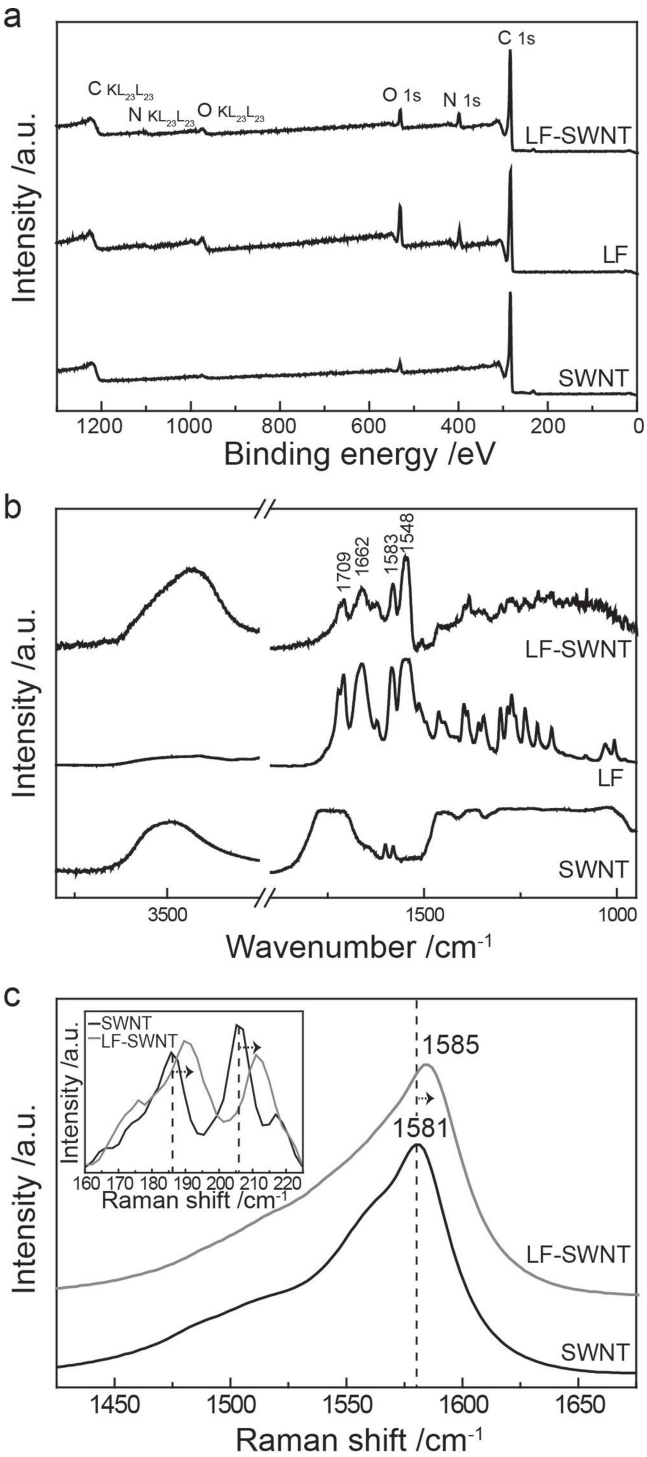

Figure 2. a. X-ray photoelectron spectroscopy survey spectra, b. Fourier transformed infrared spectra of SWNT, LF powder, and LF-SWNT hybrids. c. Raman spectra and the Radial Breathing Modes (RBMs, inset) of pristine SWNT and LF-SWNT hybrids at laser excitation 514.5 nm. Red shifting of RBMs for hybrids indicates the π–π interaction between SWNTs and LF.

cut-off voltage of 1.8 V (Figure S4) and the dense coverage of LF molecules on the surface of SWNTs that passivates the active sites in SWNTs (Figure 1d). As demonstrated in the discharge and charge profiles, the electrochemical performances of LF are markedly improved through its hybridization with SWNTs. The lithium storage capability of LF increased from 148 mAh g^{-1} (1.42 Li^+/molecule) at a current rate of C/10 (the current rate for ten-hour discharge, 0.02 A g^{-1}) for pristine LF electrodes to 204 mAh g^{-1} (1.95 Li^+/molecule, 98% of theoretical value) even at ten times higher current rate of 1C (0.2 A g^{-1}) for LF-SWNT hybrid electrodes. It is remarkable that more than 125 mAh g^{-1} of capacity (>60% of the theoretical value) could be still retained for the LF-SWNT electrodes at exceptionally high current rates of 10 A g^{-1} (corresponding to full charge/discharge in less than 46 s), as shown in Figure 3b. We noted that the hybridization of SWNTs and LF can significantly decrease the polarization (Figure 3c). In the dQ/dV plots, the separation between cathodic and anodic peaks decreased from 437 mV (for pristine LF) to 253 mV (for LF-SWNT nanohybrids) at the same current rate of 0.1 A g^{-1}. The impedance measurements in Figure 3d also indicate the remarkably enhanced kinetics of electrochemical reaction in the LF-SWNT electrode. The Nyquist plot for the LF-SWNT cell shows the decrease in the size of the semicircle at high and middle frequency range, compared to the cell with pristine LF cathode, indicating that LF-SWNT exhibits faster charge-transfer kinetics and electric responses with much lower resistance in a circuit. Note that the diffusion tail with an angle of approximately 45° from the Z axis at low-frequency region in the pristine LF cell, which corresponds to the Warburg impedance, almost disappeared in the LF-SWNT cell inferring nearly diffusion-less uptake of lithium ions of LF-SWNT. In the LF-SWNT electrodes, lithium ions can be readily supplied to the reaction sites of the individual LF molecules due to their direct exposure to the electrolyte, in contrast to the crystalline LF involving lithium diffusion through the intermolecular space formed by the stacked molecules.[26]

Figure 3e shows that the cycling performance of LF can be drastically improved by the anchorage of LF to the SWNT scaffold; after 100 cycles, the capacity of the LF-SWNT electrode was 203 mAh g^{-1}, which corresponds to 99.7% capacity retention, while the pristine LF electrode showed a capacity of only 37 mAh g^{-1} (with 34.9% capacity retention). We attribute this unprecedently stable cyclability of LF-SWNT electrodes to the effective suppression of LF dissolution into the liquid electrolyte through the π–π interactions between LF molecules and SWNTs during electrochemical cycling. According to the dissolution test of pristine LF powder and LF-SWNT nanohybrids in TEGDME, the dissolution of LF in the electrolyte was substantially suppressed after its hybridization with SWNTs (see Figure S5a for detail). More importantly, from the postmortem analysis of the electrodes after battery cycling, it was revealed that the amount of dissolved LF from the LF-SWNT electrode remained unchanged even after cycling, whereas the cycling of pristine LF electrode severely accelerated the dissolution of LF (Figure S5b,c). In addition, we believe that the improved cyclability is partially attributed to the absence of pulverization in the LF-SWNT electrodes; a large amount of lithium uptake in organic crystalline phase can accompany repeated lattice volume expansion and shrinkage, causing the disintegration of crystals (or even pulverization) deteriorating the cyclic performance, which is not the case for LF-SWNT.

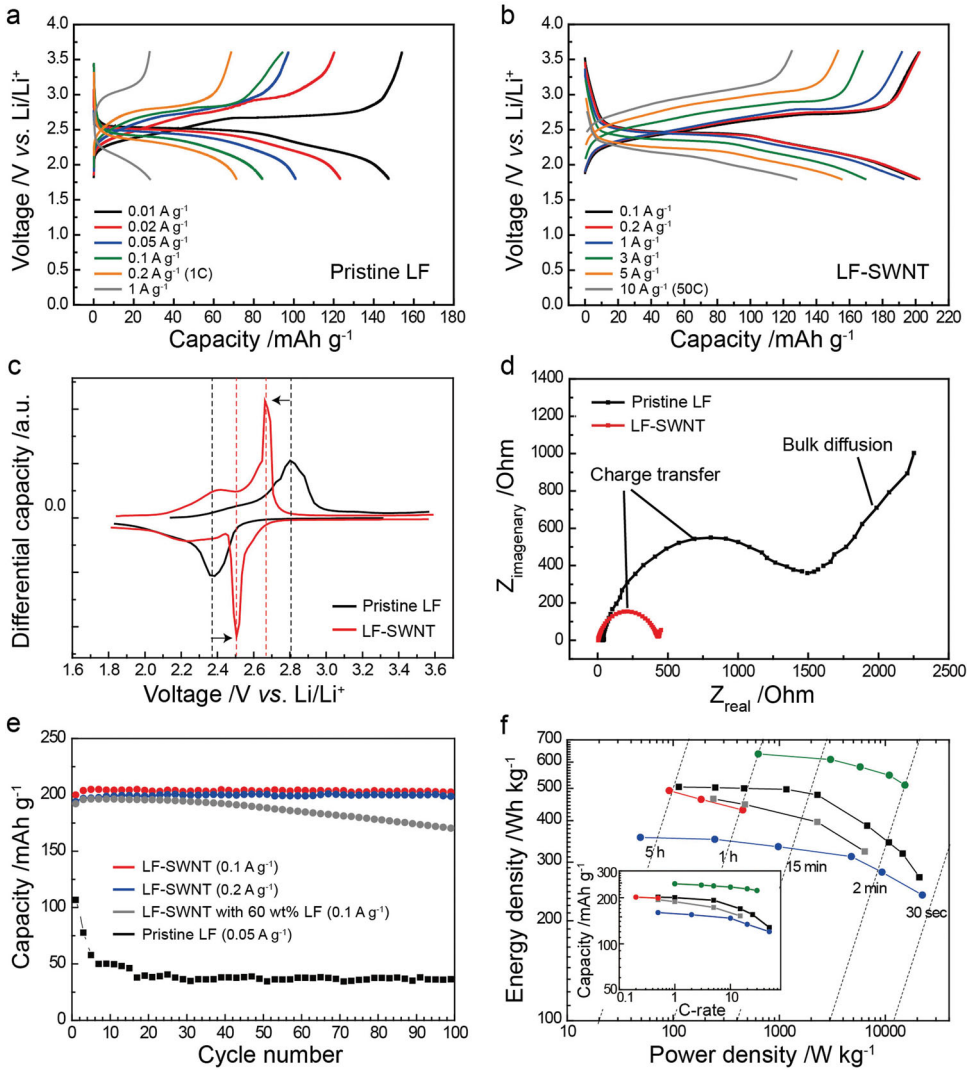

Figure 3. Electrochemical properties of LF-SWNT compared with LF as a reference. a, b. Capacity-voltage profiles of pristine LF and LF-SWNT electrodes between 1.8 and 3.6 V under various current rates. c. Differential capacity (dQ/dV) curves for pristine LF and LF-SWNT electrodes at 0.5C (0.1 A g^{-1}) rate calculated from the data in a and b. d. Nyquist plots of AC impedance test measured between 0.1 Hz and 1 MHz. e. Capacity retention of LF-SWNT electrodes and pristine LF electrodes. f. Ragone plot of LF-SWNT electrodes (-■-) and LF-SWNT electrodes of high LF content (-■-) compared with various organic-based electrodes for high power lithium rechargeable batteries. For comparison, the data of polymer-graphene composite (-●-),[27] polymer-bound PYT (-●-),[19] and polyimide (-●-)[15] are used. The inset figure shows the discharge capacity as a function of C-rate.

The trade-off between specific power and energy of LF-SWNT electrodes is represented in a Ragone plot (Figure 3f), in comparison with the state-of-the-art high-performance organic electrode materials reported in recent literatures.[15,19,27] Most lithium-battery materials exhibit a substantial decrease in specific energy with the increasing current rate, making them less useful in applications such as electric vehicles where high charge and discharge rates are required.[28] The LF-SWNT electrode clearly retains high gravimetric energy density of 500 Wh kg^{-1} over a wide range of power densities (from 0.1 kW kg^{-1} to 1 kW kg^{-1}). This result attributes to the relatively high average redox potential of LF as well as the high rate capability of LF-SWNT, as shown in the inset of Figure 3f. Even at the very high powers greater than 20 kW kg^{-1}, the LF-SWNT electrode shows a higher gravimetric energy density (272 Wh kg^{-1}) than the recent high-power electrodes for lithium rechargeable batteries, such as redox active polymer-graphene composite electrodes,[27] and polymerized electro-active organic materials (Polyimide).[15] While the specific energy and power for polymer-bound organic electrodes [pyrene-4,5,9,10-tetraone (PYT) bound to polymethacrylate] from the work by Nokami et al.[19] are relatively higher than that of the LF-SWNT electrode, the actual portion of active materials in the polymer-bound organic cathodes is only ~15 wt%. The Figure S6 illustrates this aspect in a modified Ragone plot considering the total weight of active materials, conductive agents and binder (excluding the current collector), which further highlights the outstanding performance of LF-SWNT. In LF-SWNT electrodes,

the free-standing and conductive SWNT network plays multiple roles: binder, conductive agent, and even current collector. In general, free-standing electrodes without a current collector can exhibit three to four times higher practical energy density regarding the total weight of all the components for the cathode side.[29] Therefore, our free-standing LF-SWNT electrode system promises even better performances than any other organic composites that should use an additional current collector.

To prove our hypothesis given in Scheme 1, we further fabricated LF-SWNT hybrid composites with high LF contents (60, 70 wt%) by using high concentration of LF in hybridization media, which LF contents were quantified by the elemental analysis. As shown in the SEM images, LF bulk particles were formed in the composites when the LF content exceeded the critical weight ratio during its hybridization with SWNTs through reassembly into molecular layers (Figure S7). In the electrochemical analyses for LF-SWNT with different LF contents (Figures 3,f and S8), the capacity retention and rate capability deteriorated as the LF contents in the composites increased, while their battery performances were still outstanding when compared with thoses of the pristine LF electrodes. Note that the LF-SWNT 60 wt% exhibited the best rate performances when compared with the LF-SWNT 45 wt% and the recently reported high power organic electrodes, as shown in Ragon plot based on the total mass of whole electrodes (Figure S6). These results clearly demonstrate that the rearrangement of bulk LF particles into molecular layers on SWNTs is critical for the improvement of stability and kinetics of lithium storage in LF.

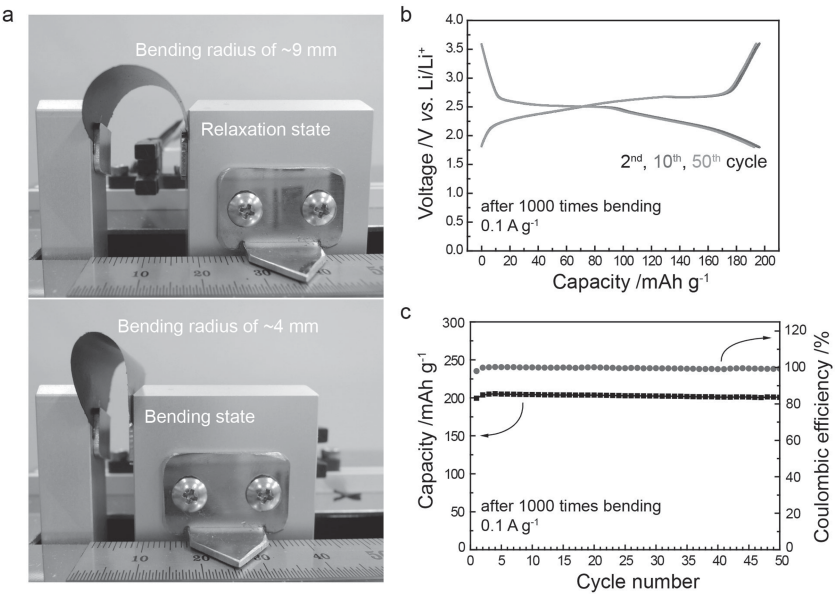

Figure 4. a. Fatigue tests of free-standing LF-SWNT electrodes on a bending stage machine. b. Capacity-voltage profiles at 0.1 A g^{-1}, c. Capacity retention and Coulombic efficiency of LF-SWNT electrodes after 1000 times of bending.

The free-standing electrode system can be also advantageous in the fabrication of bendable power sources required for flexible electronic equipment, such as rollup displays and wearable devices.[30] For such applications, reliable mechanical stability of the electrode material is critically required to maintain energy storage capability over numerous cycles of fatigue loading. In the fatigue test, as demonstrated in **Figure 4**a, the LF-SWNT paper has endured 1,000 bending cycles without causing any rupture. The rate capability and capacity retention of LF-SWNT electrodes were perfectly maintained after 1000 times of bending and relaxation (Figure 4a, b). The origin of high mechanical stability of LF-SWNT electrodes can be attributed to the interpenetrating network structure of SWNTs and their stable contact with the anchored LF molecules during the repeated bending. Moreover, the separation of active materials from the stiff metal current collector, which often happens in conventional electrodes, is prevented in the free-standing nanohybrid electrodes not having any current collector.

We further examined general applicability of our nanohybridization approach for other aromatic redox molecules. Firstly, we tested vitamin B_2 (also known as riboflavin) which has a ribityl side chain rather than a methyl group in lumiflavine. Riboflavin (RF) was successfully incorporated within SWNTs through the same procedure as that of LF hybridization (See Figure S9). RF-SWNT exhibited nearly perfect capacity retention (approximately 100%) after 100 cycles with high Coulombic efficiency over 99.65% (**Figure 5**a), which is remarkable considering the poor cyclability of the pristin RF electrode (Figure S10a). Furthermore, anthraquinone (AQ, $C_{14}H_8O_2$), one of the most well-known quinone-based cathode materials,[14,31] was also able to hybridize with SWNTs under the same process. Although AQ has been reported as a high capacity electrode with its theoretical capacity of 257 mAh g^{-1} utilizing two lithium ions in its conjugated carbonyl groups, poor cyclability and slow kinetics have so far shadowed its importance as a battery electrode (Figure S10b).[14] Nevertheless, after nanohybridization, AQ-SWNT demonstrated capacity retention of 98.25% after 50 cycles with high Coulombic efficiency above 99.80% (Figure 5b). As shown in insets of Figure 5a and 5b, both nanohybrid electrodes, RF-SWNT and AQ-SWNT, could deliver high rate capability. These results signify the possibility of exploiting our simple nanohybridization strategy for various redox-active organic molecules to achieve high performance organic electrodes for lithium rechargeable batteries.

In summary, we have successfully developed flexible, free-standing organic electrodes via a facile nanohybridization strategy by non-covalently immobilizing redox-active aromatic molecules onto the surface of SWNTs by π–π interactions. The molecular rearrangement of LF from bulk crystalline particles into a molecular layer wrapping around SWNTs allowed the fast kinetics for lithium storage, while the stable contact between electro-active LF and the SWNT scaffolds afforded a high electronic conducting path. The binder-, additive-, current collector-free organic-SWNT nanohybrids exhibited greatly improved energy storage properties such as specific capacity, cyclic stability, and rate capability. High gravimetric energy density up to 500 Wh kg^{-1} was achieved within 25-minute discharge.

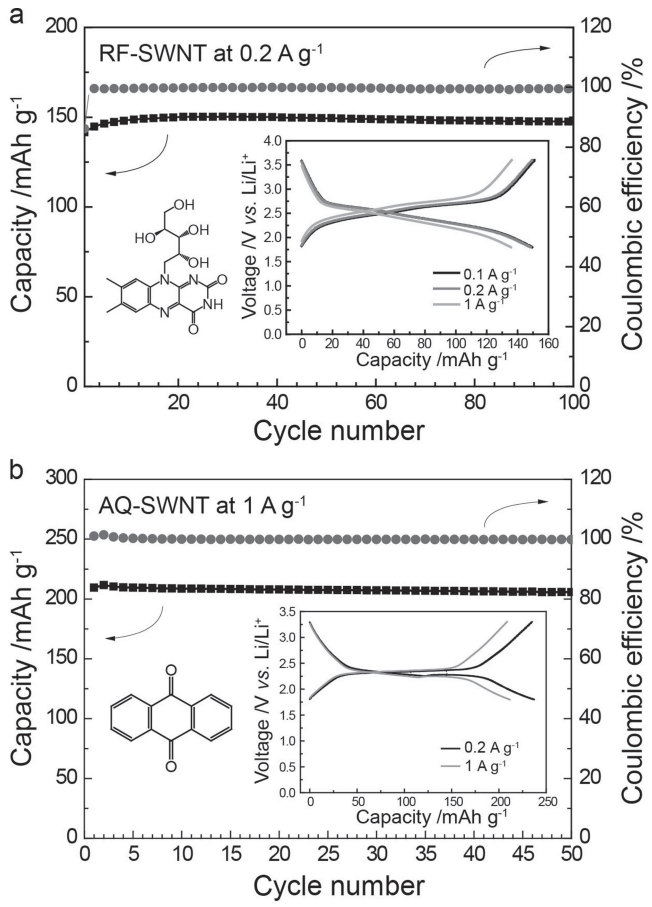

Figure 5. a. Capacity retention and Coulombic efficiency of the RF-SWNT at 0.2 A g^{-1}. Inset shows the discharge-charge profiles of RF-SWNT electrodes at rates of 0.1 A g^{-1}, 0.2 A g^{-1}, and 1 A g^{-1} between 1.8 and 3.6 V. b. Capacity retention and Coulombic efficiency of AQ-SWNT at 1 A g^{-1}. Inset shows the discharge-charge profiles of AQ-SWNT electrodes at rates of 0.2 A g^{-1}, and 1 A g^{-1} between 1.6 and 3.3 V.

Even at the very high powers greater than 20 kW kg^{-1}, a high gravimetric energy density (272 Wh kg^{-1}) was achieved, which is comparable to that of the most state-of-the-art organic electrodes ever reported. The electrochemical properties of the nanohybrid electrodes were also perfectly retained even after the repeated mechanical bending posing its potential application to flexible energy storage systems. We expect that the versatility of our simple approach can be easily extended to various unexplored aromatic molecules, which can bring the green energy materials into reality in the near future.

Experimental Section

Synthesis of nanohybrid electrodes: All reagents were purchased from Sigma-Aldrich unless otherwise specified. A mixture of SWNTs (5 mg) and lumiflavine (4.5 mg) was added to acetone (20 ml). The solution was homogenized with an ultrasonic Vibra Cell VCX 750 homogenizer (Sonics & Materials Inc., USA) for 10 min (2 sec on, 1 sec off), followed by sonication for 8 hours at 300 W intensity. Then, the solution was filtered through a Whatman Anodisc membrane of 0.1 μM pore size, followed by vacuum drying. The resulting interwoven and mechanically robust LF-SWNT film was easily removed from the membrane filter. The LF-SWNT film was directly utilized as the free-standing cathode without any further inclusion of binder, additives, and a current collector. For riboflavin-SWNT synthesis, riboflavin (3 mg) was hybridized with SWNT (5 mg) in deionized (DI) water (20 ml) following the same procedure as mentioned above. For anthraquinone-SWNT preparation, anthraquinone (15 mg) was mixed with SWNTs (5 mg) in acetone (20 ml) and followed the same procedure above.

Characterization: The morphologies of LF-SWNT were analyzed using an S-4800 field-emission scanning electron microscope (SEM) (Hitachi High-technologies Co., Japan) and a Tecnai G2 F30 transmission electron microscope (TEM) (FEI Co., Netherlands). The electron diffraction patterns were obtained on a JEM-3011 in-situ TEM (JEOL Ltd., Japan). Immobilization of LF on the SWNTs scaffolds were characterized by X-ray photoelectron spectroscopy (XPS) using a Thermo VG Scientific Sigma Probe spectrometer (U.K.) equipped with a microfocus monochromated X-ray source (90 W) and by Fourier transform infrared spectroscopy (FTIR) using FT/IR-4200 (Jasco Inc., Japan) at a resolution of 2 cm^{-1} under argon atmosphere. The π–π interactions of LF and SWNTs were investigated using a LabRAM Aramis dispersive Raman microscope (Horiba Jobin Yvon, France) at an excitation laser of 514.5 nm. The active contents in nanohybrids were analyzed using an EA1110-FISONS elemental analyzer (ThermoQuest Italia S.P.A., Italy) and a TG 209 F3 thermogravimetry analyzer (NETZSCH, Germany). In the fatigue test, one end of the as-prepared LF-SWNT film (~33 mm diameter) was gripped to a fixed side with a flat magnet, and the other end was attached to a mobile bar on a custom-made bending stage machine. The bending radius of the film was repeatedly varied from 9 mm to 4 mm by constant speed of 1 cycle per second 1,000 times.

Electrochemical measurements: Electrochemical performances of the organic electrodes were measured versus pure Li metal foil (Hohsen Corp., Japan) in coin-type cells (CR2016). Pristine LF, RF, and AQ electrodes were fabricated by mixing 40 wt% active materials, 40 wt% carbon black (Super P) and 20 wt% PTFE (polytetrafluoroethylene) binder. Organic compounds-SWNT hybrid electrodes were used as prepared without further treatments. A porous polypropylene membrane (Celgard 2400) was used as a separator. 70 μl of 1 M $LiPF_6$ in tetraethylene glycol dimethyl ether (TEGDME) was used as the electrolyte for each battery. The cells were assembled in an inert atmosphere within an Ar-filled glove box. The galvanostatic discharge and charge measurements were carried out at various current densities from C/20 to 50C (1C rate = 0.2 A g^{-1}) in the voltage ranges of 1.8–3.6 V on a battery test system (Won-A Tech, Korea) at 25 °C. The electrochemical impedance spectroscopy (EIS) analysis were carried on the pristine coin cells made with LF and LF-SWNT electrodes in the frequency range 1 MHz – 0.1 Hz with an AC signal amplitude of 10 mV.

Ex situ Electrolyte analysis: For ex situ UV/Vis absorbance analyses, all of the cell components except the positive electrodes were recollected from the disassemble coin cells and stored in 2 mL of TEGDME solvent. The cells for the ex situ analyses were rested for 24 hours or discharged and charged for a cycle at C/10 rate. UV/Vis absorbance spectra of the diluted electrolytes were obtained using a V/650 spectrophotometer (Jasco Inc., Japan) in the range of 380–540 nm.

Supporting Information

Supporting Information is available from the Wiley Online Library or from the author.

Acknowledgements

This study was supported by the National Research Foundation through Converging Research Center (2010–50207), Intelligent Synthetic Biology Center of Global Frontier Project (2011–0031957),

and NLRL Program (NRF-2013R1A2A1A05005468), Republic of Korea. This work was supported by Institute for Basic Science(IBS). This work was also supported by the Human Resources Development program (20124010203320) of the Korea Institute of Energy Technology Evaluation and Planning (KETEP) grant funded by the Korea government Ministry of Trade, Industry and Energy, the Converging Research Center Program through the Ministry of Education, Science and Technology(2013K000293), and the development of organic electrode materials for lithium ion batteries project (UE1240220D) funded by the Agency for Defense Development (ADD), Republic of Korea.

Received: October 8, 2013
Revised: November 17, 2013
Published online: February 1, 2014

[1] M. Armand, J. M. Tarascon, *Nature* **2008**, *451*, 652.
[2] P. Poizot, F. Dolhem, *Energy Environ. Sci.* **2011**, *4*, 2003.
[3] J. M. Tarascon, *ChemSusChem* **2008**, *1*, 777.
[4] P. Yang, J.-M. Tarascon, *Nat. Mater.* **2012**, *11*, 560.
[5] H. Chen, M. Armand, G. Demailly, F. Dolhem, P. Poizot, J. M. Tarascon, *ChemSusChem* **2008**, *1*, 348.
[6] W. Walker, S. Grugeon, O. Mentre, S. p. Laruelle, J.-M. Tarascon, F. Wudl, *J. Am. Chem. Soc.* **2010**, *132*, 6517.
[7] H. Chen, M. Armand, M. Courty, M. Jiang, C. P. Grey, F. Dolhem, J.-M. Tarascon, P. Poizot, *J. Am. Chem. Soc.* **2009**, *131*, 8984.
[8] M. Lee, J. Hong, D.-H. Seo, D. H. Nam, K. T. Nam, K. Kang, C. B. Park, *Angew. Chem., Int. Ed.* **2013**, *52*, 8322.
[9] Y. Liang, Z. Tao, J. Chen, *Adv. Energy Mater.* **2012**, *2*, 742.
[10] M. Armand, S. Grugeon, H. Vezin, S. Laruelle, P. Ribiere, P. Poizot, J. M. Tarascon, *Nat. Mater.* **2009**, *8*, 120.
[11] D. J. Kim, S. H. Je, S. Sampath, J. W. Choi, A. Coskun, *RSC Adv.* **2012**, *2*, 7968.
[12] B. Genorio, K. Pirnat, R. Cerc-Korosec, R. Dominko, M. Gaberscek, *Angew. Chem., Int. Ed.* **2010**, *49*, 7222.
[13] X. Han, C. Chang, L. Yuan, T. Sun, J. Sun, *Adv. Mater.* **2007**, *19*, 1616.
[14] Z. Song, H. Zhan, Y. Zhou, *Chem. Commun.* **2009**, 448.
[15] Z. Song, H. Zhan, Y. Zhou, *Angew. Chem., Int. Ed.* **2010**, *49*, 8444.
[16] Y. Morita, S. Nishida, T. Murata, M. Moriguchi, A. Ueda, M. Satoh, K. Arifuku, K. Sato, T. Takui, *Nat. Mater.* **2011**, *10*, 947.
[17] Y. Hanyu, I. Honma, *Sci. Rep.* **2012**, *2*, 453.
[18] W. Guo, Y.-X. Yin, S. Xin, Y.-G. Guo, L.-J. Wan, *Energy Environ. Sci.* **2012**, *5*, 5221.
[19] T. Nokami, T. Matsuo, Y. Inatomi, N. Hojo, T. Tsukagoshi, H. Yoshizawa, A. Shimizu, H. Kuramoto, K. Komae, H. Tsuyama, J.-i. Yoshida, *J. Am. Chem. Soc.* **2012**, *134*, 19694.
[20] S. Y. Ju, J. Doll, I. Sharma, F. Papadimitrakopoulos, *Nat. Nanotechnol.* **2008**, *3*, 356.
[21] S. Y. Ju, W. P. Kopcha, F. Papadimitrakopoulos, *Science* **2009**, *323*, 1319.
[22] N. R. Tummala, B. H. Morrow, D. E. Resasco, A. Striolo, *ACS Nano* **2010**, *4*, 7193.
[23] G. Wille, M. Ritter, R. Friedemann, W. Mäntele, G. Hübner, *Biochemistry* **2003**, *42*, 14814.
[24] S. Gotovac, H. Honda, Y. Hattori, K. Takahashi, H. Kanoh, K. Kaneko, *Nano Lett.* **2007**, *7*, 583.
[25] R. Voggu, C. S. Rout, A. D. Franklin, T. S. Fisher, C. N. R. Rao, *J. Phys. Chem. C* **2008**, *112*, 13053.
[26] D.-H. Seo, H. Kim, H. Kim, W. A. Goddard, K. Kang, *Energy Environ. Sci.* **2011**, *4*, 4938.
[27] Z. Song, T. Xu, M. L. Gordin, Y. B. Jiang, I. T. Bae, Q. Xiao, H. Zhan, J. Liu, D. Wang, *Nano Lett.* **2012**, *12*, 2205.
[28] K. Kang, Y. S. Meng, J. Bréger, C. P. Grey, G. Ceder, *Science* **2006**, *311*, 977.
[29] L.-F. Cui, L. Hu, J. W. Choi, Y. Cui, *ACS Nano* **2010**, *4*, 3671.
[30] H. Gwon, H.-S. Kim, K. U. Lee, D.-H. Seo, Y. C. Park, Y.-S. Lee, B. T. Ahn, K. Kang, *Energy Environ. Sci.* **2011**, *4*, 1277.
[31] W. Xu, A. Read, P. K. Koech, D. Hu, C. Wang, J. Xiao, A. B. Padmaperuma, G. L. Graff, J. Liu, J.-G. Zhang, *J. Mater. Chem.* **2012**, *22*, 4032.